Applied Energy 306 (2022) 118005

Contents lists available at ScienceDirect

Applied Energy

journal homepage: www.elsevier.com/locate/apenergy

Performance improvement of variable-angle annular thermoelectric generators considering different boundary conditions

Zebin Weng [a], Furong Liu [a], Wenchao Zhu [a,b], Yang Li [a,c], Changjun Xie [a,b,*], Jian Deng [a], Liang Huang [a,*]

[a] School of Automation, Wuhan University of Technology, Wuhan 430070, China
[b] Hubei Key Laboratory of Advanced Technology for Automotive Components, Wuhan University of Technology, Wuhan 430070, China
[c] Department of Electrical Engineering, Chalmers University of Technology, Gothenborg 41576, Sweden

HIGHLIGHTS

- A new model of annular thermoelectric generator with variable-angle PN legs.
- Theoretical relationship of output performance between CATEG and VATEG.
- A 3D model of the VATEG by COMSOL to investigate the thermal stress and discuss the influence of shape difference.
- A 35% higher of output performance, while 30% higher of maximum thermal stress under the same volume.

ARTICLE INFO

Keywords:
Variable-angle annular thermoelectric generator (VATEG)
Finite element method
Shape factor
Thermal stress
Energy efficiency
Heat recovery

ABSTRACT

Practical applications of thermoelectric generators are impeded by their low thermoelectric conversion efficiency, and improving the efficiency is vital for the advancements of thermoelectric technology. In this paper, a novel method is proposed for the performance analysis and improvement of the annular thermoelectric generators with variable-angle *PN* legs (VATEGs). The influence of the *PN* leg angle on the output performance of the VATEG is investigated by introducing an angle function. Given the volume of the *PN* legs, the relationship of output performance between the VATEG and traditional constant-angle ATEG (CATEG) is established under different boundary conditions based on a proposed generic model of VATEG. The results are verified numerically using the finite element method. Using the model, it is shown that the output performance of the VATEG is significantly affected by the shape of the *PN* leg. Finally, the thermal stress on the *PN* leg is next investigated using a high-fidelity 3D model of the variable-angle *PN* legs implemented in COMSOL, and it is found that the shape difference has a considerable influence on the thermal stability of VATEG. Under the condition of constant heat flux on the hot side and constant temperature on the cold side of the thermoelectric modules, it shows that when the radius factor is 2, the output performance can be improved by 35% with the designed VATEG, at the expense of 30% higher maximum thermal stress on the *PN* legs.

1. Introduction

Global energy crisis and environmental issues demand more sustainable and clean energy with improved energy conversion efficiency [1]. Amongst various green energy harvest candidates, a thermoelectric generator (TEG) couples thermal field and electric field to generate electrical power from heat sources according to the Seebeck effect [2], and it is a promising technology due to its low-cost production, environment-friendly operation, and free of moving parts [3]. TEGs can be potentially used in various applications. For example, the thermal energy in the waste heat of automobile exhaust gas can be recovered using TEGs [4]. The heat in solar photovoltaic panels can be utilized for TEGs to generate additional electricity to supply remote villages [5]. In biomedicine, TEGs can be used for micro-heat energy recovery by converting human waste heat to electricity for establishing a self-powered human health detection system [6]. In artificial intelligence and aviation, waste heat can be recovered by developing isotope radioactive TEGs [7] or micro thermoelectric components [8].

Unfortunately, practical applications of TEGs are impeded by the low

* Corresponding authors at: School of Automation, Wuhan University of Technology, Wuhan 430070, China (C. Xie).
E-mail addresses: jackxie@whut.edu.cn (C. Xie), huangliang@whut.edu.cn (L. Huang).

https://doi.org/10.1016/j.apenergy.2021.118005
Received 22 June 2021; Received in revised form 25 August 2021; Accepted 2 October 2021
Available online 11 October 2021

Nomenclature

Symbols

V	volume (m^3)
m	exponent coefficient of angle function
R_t	internal resistance (Ω)
K	thermal conductance (W/K)
R	electrical resistance (Ω)
r_h	inner radius of thermocouple (mm)
r_c	outer radius of thermocouple (mm)
T	temperature (K)
I	current (A)
H	length of thermocouple (mm)
f	shape factor
r	radius of thermocouple (m)
S	number of finite element discretization
n	number of thermocouples
P	power (W)
Q	heat flow (W)
Q_{in}	heat absorbed by thermocouple module (W)
Q_{out}	heat released from thermocouple module (W)
q	scaling coefficient of angle function
h	convective heat transfer coefficient (W m^{-1} K^{-1})
A	cross-sectional area (m^2)
T_e	ambient temperature (K)
U	Seebeck voltage (V)

Greek symbols

α	Seebeck coefficient (V/K)
λ	thermal conductivity (W/(m K))
σ	electrical conductivity (S/m)
δ	thickness of thermocouple (mm)
θ	angle of PN legs (rad)
ξ	heat flux (W m^{-2})
η	conversion efficiency (%)
ρ	electrical resistivity (m/S)

Superscript

k	index of elementary unit ($k = 1,2,\cdots, S$)

Subscript

χ	*P*-type or *N*-type leg
e	ceramic layer
0	parameters of CATEG
P	*P*-type leg
N	*N*-type leg
L	external load
h	hot side of *PN* leg
c	cold side of *PN* leg

thermoelectric conversion efficiency, and improving the efficiency is vital for the advancements of thermoelectric technology. The factors that influence the thermoelectric efficiency and the output power of TEGs can be generally divided into internal and external factors. *Internal factors* are associated with the thermoelectric materials used in TEG devices. To assess how the performance of TEG is affected by the internal factors, the figure of merits *ZT*, a dimensionless parameter, is commonly used in the literature, and a larger *ZT* indicates superior performance. Defined by $ZT = \alpha^2\sigma T/\lambda$, the figure of merits is a function of the Seebeck coefficient α, electrical conductivity σ, operating temperature T, and the thermal conductivity λ [9]. Since these parameters are often intercorrelated, it is challenging to obtain optimal performance by adjusting them independently. In the literature, the *ZT* of common thermoelectric materials ranges from 1 to 1.8 [10], and some studies show that the *ZT* can achieve over 2 [11]. The *ZT* of thermoelectric materials with nanostructures can be increased to 1.7 [12]. With well-developed material processing technology, a *ZT* of 1.8 can be achieved [13]. If the *ZT* can be increased further to 3, the thermoelectric conversion efficiency can exceed 30%, which is promising for practical applications [14]. Thermoelectric materials with *ZT* over 4 can receive substantial commercial interest in the future. Hence, the exploration of high *ZT* is of great significance [15]. Some materials, such as ZnO [16] and graphene [17], have relatively high electrical conductivity without processing. Other materials demand particular processing procedures to increase the electrical conductivity or reduce the thermal conductivity. For example, Rogl *et al.* [18] refined the skutterudites from commercial powders by cold pressing and high-pressure torsion at 850 K. With this method, the thermal conductivity of skutterudites can be significantly reduced at the expense of slightly reduced electrical conductivity, leading to a high figure of merits $ZT = 2.1$. Doping other ingredients enables further improvement on *ZT*. For instance, Zhao *et al.* [19] concluded that $ZT = 1.34$ could be obtained by doping sodium in tin selenide samples. In addition, searching for thermoelectric materials with high *ZT* values, such as Zintl phases [20] and half-Heusler alloys [21], is also an effective way to enhance thermoelectric efficiency.

On the other hand, the operating temperature of *PN* legs, shape matching between the heat source and the heat exchanger, and the geometric parameters belong to *external factors*. Some studies have attempted to match the optimal operating temperatures with different materials via segmented [22] or staged TEGs [23]. For instance, Chen *et al.* [24] designed a segmented TEG system. Compared to conventional TEGs, the output power and efficiency of the TEG system can be improved by 21.94% and 14.05%, respectively. In a different study, Karana *et al.* [25] showed that the overall efficiency of a segmented TEG can be increased by 5%. El-Genk *et al.* [26] proposed a segmented TEG with skutterudites, and its thermoelectric efficiency can reach 14.7% when the cold and hot side temperatures are 573 K and 300 K, respectively. In addition, the nonlinear physical properties of the materials are taken into consideration to improve the performance of the TEGs further. In fact, the assumption of constant physical properties is only applicable to micro TEGs or wearable thermoelectric energy harvest devices with ignorable temperature gradients. Since a large temperature gradient exists in most industrial applications, the dependence of the material parameters on local temperature should be considered during the design of the TEG system. The impact of nonuniform temperature distribution on the output performance of the *PN* legs can be investigated using the finite element method (FEM) [27]. For example, Meng *et al.* [28] used a 1D numerical model to study the multi-irreversibility effects of TEGs. Thermoelectric materials with nonlinear parameters can also be modeled with 3D commercial software for numerical simulation, such as FLUENT, COMSOL, and ANSYS [29].

The shape of the heat exchanger is the second external factor that needs to be properly considered. Well-matched heat source and heat exchanger can effectively reduce the heat loss arising from the contact impedance. For cylindrical heat sources such as exhaust pipes in automobiles, the TEG is usually designed into annular or ring-annular to match the cylindrical heat sources [30]. Bauknecht *et al.* [31] investigated the performance of an ATEG under the condition of nonuniform temperature distribution, and it was shown that the output performance can be significantly improved. Shen *et al.* [32] studied both the annular and the flat TEGs by developing a steady-state model and revealed that the governing equations of both designs are similar except for the mathematical expressions of the resistance and thermal conductivity. Hence, an ATEG can be converted into a flat TEG to evaluate its

performance. Moreover, the research interest in flexible TEGs is growing in recent years, and these TEGs are mainly used in wearable devices to match the complex structure of the heat source, i.e., the human body [33]. Cui *et al.* [34] examined several aspects in designing a flexible wearable TEG, such as the convective heat transfer coefficient between the thermal layer and the environment, as well as the contact thermal resistance between the thermal layer and the skin. Their results exhibited that the degree of flexible bending is associated with the open-circuit voltage (OCV), and the maximum power density can be achieved by properly selecting the length of the hot spot layer. The shape of TEG can also affect the external thermal resistance and output power of the TEG. For example, Kim *et al.* [35] proposed a direct contact TEG to reduce the contact thermal resistance, resulting in a 132% increase in the output power. Apart from the steady-state performance, there are also many studies on the transient heat transfer process of segmented ATEGs, and the research objective is usually to test the mechanical features of the materials. For example, Asaadi *et al.* [36] investigated rectangular, triangular, and sinusoidal pulsed inputs to study the performance of an ATEG, and compared the results with the steady-state performance under the same operating conditions. The authors concluded that all these pulse heating strategies could enhance the efficiency of ATEG, while the rectangular pulse heating strategy is the best with which the efficiency can be improved by 249.36%. Similarly, Fan *et al.* [37] analyzed the thermoelectric and mechanical properties of an ATEG under both transient and steady-state conditions. Their results showed that the output power can be increased by 18.3% with a segmented structure, and the maximum von Mises stress can be reduced by 12.5%. Shittu *et al.* [38] studied the electrical and mechanical characteristics of segmented and asymmetric thermoelectric legs in the steady-state and transient, and the optimized geometric parameters of the legs were obtained. The optimized TEG output power was increased by 117.11% with rectangular pulse heating inputs, and the thermal stress of an N-type asymmetric leg is 39.21% smaller than that of a P-type symmetric leg on the cold side. Samson *et al.* [39] investigated the thermoelectric and mechanical properties of two ATEGs based on bismuth telluride and skutterudite. The authors showed that when the temperature difference is above 200 K, the efficiencies of the segmented ATEG are 21.7% and 82.9% higher than the designs without segmentation, and increasing the leg length can effectively reduce the thermal stress and improve the electrical performance.

When the materials and segmentation method has been determined, optimization on various *geometric parameters* of the *PN* legs can play an important role in achieving high TEG performance. A large body of literature exists to investigate the geometric parameter optimization of TEGs from both technical and economic aspects [40–42]. Furthermore, different boundary conditions applied to the model can affect optimization results. Fan *et al.*[43] studied the influence of the variations of geometric parameters on output power and energy conversion efficiency under different thermal boundary conditions. It shows that the efficiency is unchanged at the boundary condition of constant temperature and inversely proportional to the cross-sectional area of legs under the boundary condition of constant heat transfer coefficient. He *et al.* [44] proposed a 1D model of the TEG based on the hill-climbing algorithm, considering the size of the hot leg. It was verified by the 3D numerical simulation that for any leg length, the maximum output power always increases with the increase of leg area. Chen *et al.* [42] used the genetic algorithm to optimize the cross-sectional area and the length of legs, with conversion efficiency being the objective function. Under a fixed temperature difference of 40 K, the output power and efficiency corresponding to the optimized cross-sectional area and length are 51.9% and 5.4% higher than the original TEG design.

Conventionally, *PN* legs are designed with a fixed leg angle. Recently, there is growing interest in designing non-conventional *PN* legs. Fabián-Mijangos *et al.* [45] designed a thermoelectric module with a *PN* leg in an asymmetric truncated square pyramid shape. Compared to the traditional design, the thermoelectric quality factor can be doubled

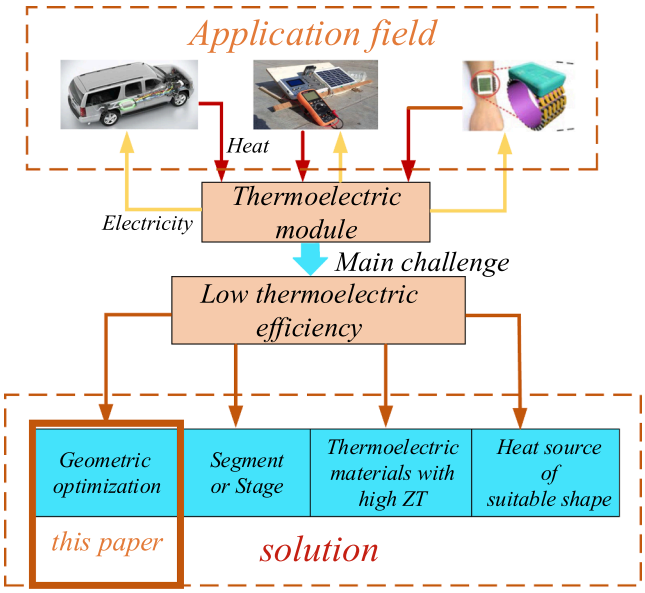

Fig. 1. Overview of application fields and research directions of thermoelectric generators for thermal energy recovery.

under the same operating condition. Sahin *et al.* [46] showed that legs with linearly varying cross-sectional areas in the leg length direction could reduce the output power. In fact, the cross-sectional area can be designed to be changed linearly, exponentially [47], or irregularly [48] in the leg length direction. Bengisu *et al.* [49] conducted numerical simulations with trapezoids-shaped and hourglass-shaped *PN* legs and considered different boundary conditions. The results showed that the hourglass-shaped leg has twice as much potential and maximum power as the traditional *PN* leg. At the same time, it showed that the influence of boundary conditions should be considered when choosing the best shape. Zhang *et al.* [50] introduced the formula of thickness variation along the leg length direction $\delta(r) = a_m r^m$ to discuss the influence of variable cross-sectional areas on the output characteristics of an ATEG, and the authors concluded that the power per unit mass could be maximized when $m = -1$. Liu *et al.* [51] obtained the relationship between the thermal resistances of variable cross-section leg and fixed cross-section leg for flat-plate TEGs. It was found that the conversion efficiency can be improved with variable cross-sections, and the output power depends on both the boundary conditions and the shape factor. However, the derived expression had not been verified with different materials and at different working temperatures. Ali *et al.* [52] optimized the cross-sectional area of the exponentially changed leg by introducing a dimensionless geometric parameter. It was found that although the output efficiency can be improved, there is a tradeoff between the efficiency and the output power. However, this paper does not quantitatively compare the output performance of the proposed design with the traditional TEG. Liu *et al.* [53] developed a solar TEG model taking into account the subsection and asymmetry of thermoelectric legs. It concluded that with the subsection, the output power can be increased by 14.9%, and with the optimal cross-sectional area of the *PN* legs, the output power can be increased by 16.6%. The performance of this design was evaluated using a 3D multi-physics thermoelectric model, whereas the thermal stress and thermal stability of the thermoelectric structure was not considered for different cross-sectional areas.

The abovementioned research background and research directions are summarized in Fig. 1. Since well-selected geometric parameters of the *PN* legs can effectively improve the thermoelectric conversion efficiency, the primary research objective of this paper is to improve the thermoelectric conversion performance from the perspective of geometric parameter optimization. Although extensive efforts have been devoted to the research on geometric parameter optimization, several

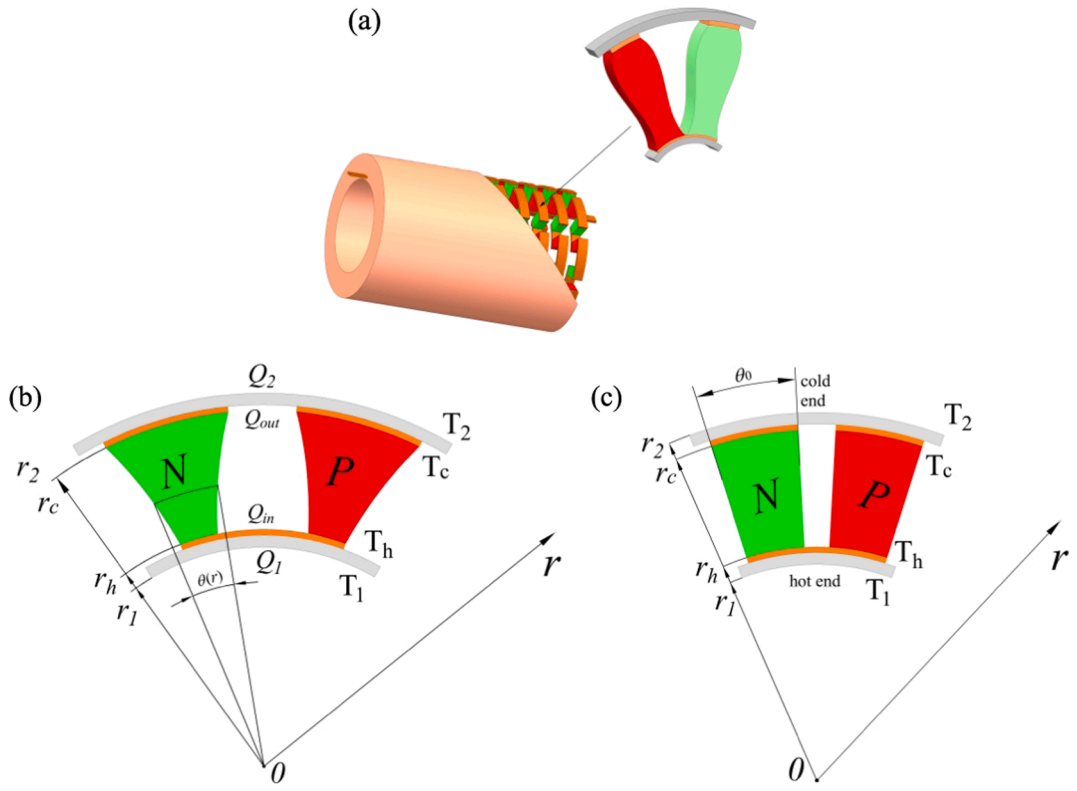

Fig. 2. Schematic diagrams of the proposed VATEG. (a) 3D view of VATEG and a *PN* leg with variable leg angles. (b) 2D view of a pair of *PN* legs with variable leg angles. (c) 2D view of *PN* legs with a fixed leg angle of a CATEG.

aspects of practical consideration are rarely investigated in the existing studies. First, it is necessary to pay attention to the temperature distribution of *PN* legs if the cross-sectional areas are variable [54]. For a practical system, examining whether the designed shape difference can cause local over-temperature is essential to avoid potential damage on thermoelectric material, although the procedure is usually ignored in many existing works. Second, we notice that there is a lack of study on the influence of the change of the cross-section area on the material and structural stability for practical use. In addition, theoretical derivation and analysis based on a 3D model with the leg shape change in the ATEG are both rarely investigated. In order to fill the research gaps, this paper proposes a new ATEG design with variable-angle *PN* leg (VATEG) and establishes a generic geometric ATEG model to describe the change of *PN* leg angle in the leg length direction. Specifically, given the leg volume, the relationship between the physical parameters of VATEG and the corresponding constant-angle ATEG (CATEG) is first obtained from theoretical analysis. The angle function of *PN* legs is next derived with different boundary conditions to compare the output performance, and the results are verified using a high-fidelity 3D model implemented in COMSOL. Finally, to confirm whether the stability of *PN* legs material is affected by the shape difference, the developed 3D model is utilized to study the temperature distribution of the proposed VATEG and the thermal stress on *PN* legs. Note that the proposed model is generic, and the analysis can be extended to obtain the optimized design with other boundary conditions that are not studied in the present investigation. The contributions of the proposed method are summarized as follows:

(1) A generic ATEG model is first developed by introducing a two-parameter angle function to analyze and simulate the heat recovery process for practical application.
(2) Under the assumption of the same volume of *PN* legs, the relationship between the resistance and thermal conductance of the *PN* leg is established for the first time, and the two parameters in the angle function were characterized with a proposed shape factor.
(3) In order to guarantee the suitability of the proposed research method for other application fields, different scenarios are simulated and verified by considering different boundary conditions on the cold and the hot sides. The relationship of the output performance between the proposed VATEG and the traditional ATEG is derived under different boundary conditions.
(4) Thermal stress and voltage distribution under different boundary conditions and leg lengths are first investigated using a 3D model, and the results were compared with the traditional ATEG to study how the shape of *PN* leg can affect the thermal stress.

2. Model description and theoretical analysis

Fig. 2(a) shows the 3D structure of the proposed VATEG, where the *PN* legs angle along the leg length direction is not designed as a constant. Fig. 1(b) and (c) are the schematic diagrams of the proposed and the conventional designs of the *PN* legs, respectively. For the ease of model development and analysis, the following assumptions are made in this work.

(1) All surfaces are insulated except for the hot and cold surfaces;
(2) Only the heat transfer along the leg length direction is considered;
(3) The Thomson effect is not considered;
(4) The electrical resistance and the contact thermal resistance of the copper sheets are ignored;
(5) The heat loss due to radiation in all directions is neglected;
(6) The *P*-leg and the *N*-leg possess symmetrical geometric structures;
(7) The leg volume and the leg length of the proposed design are both the same as those in the conventional design.

2.1. Shape factor of PN legs

As shown in Fig. 2(b), the inner radius and the outer radius of the *PN* legs are denoted by r_h and r_c, respectively, and the leg length is $H = r_c - r_h$. In contrast to using a constant leg angle θ_0 in the conventional CATEG, the leg angle of a VATEG varies with respect to the radial coordinate r, denoted by $\theta(r)$. The expression of $\theta(r)$ can be derived by equalizing the leg volumes of CATEG and VATEG, i.e.,

$$\int_{r_h}^{r_c} r \times \theta(r) \times \delta dr = \int_{r_h}^{r_c} r \times \theta_0 \times \delta dr = \frac{\theta_0 \cdot r_h^2 \cdot (Sr^2 - 1)}{2} \times \delta \tag{1}$$

where δ is the thickness of *PN* legs and *Sr* is the radius ratio defined as

$$Sr = r_c / r_h \tag{2}$$

For the CATEG, the resistance and the thermal conductance of *PN* legs are calculated by [55]

$$R_{leg,0} = \int_{r_h}^{r_c} \frac{dr}{\sigma \cdot \theta_0 \cdot r \cdot \delta} = \frac{ln(Sr)}{\sigma \cdot \theta_0 \cdot \delta}$$
$$K_{leg,0} = \frac{\lambda \cdot \theta_0 \cdot \delta}{ln(Sr)} \tag{3}$$

where σ and λ are the electrical conductivity and the thermal conductivity of *PN* legs, respectively. Note that the subscript '0' indicates the quantity for the corresponding CATEG design in this work.

Similarly, for the VATEG, with (2) and (3), the resistance and the thermal conductance are

$$R_{leg} = \int_{r_h}^{r_c} \frac{dr}{\sigma \cdot \theta(r) \cdot r \cdot \delta} = \left(\frac{\theta_0}{ln(Sr)} \int_{r_h}^{r_c} \frac{dr}{\theta(r) \cdot r}\right) \cdot R_{leg,0}$$
$$K_{leg} = \frac{1}{\int_{r_h}^{r_c} \frac{dr}{\lambda \cdot \theta(r) \cdot r \cdot \delta}} = \frac{K_{leg,0}}{\left(\frac{\theta_0}{ln(Sr)} \int_{r_h}^{r_c} \frac{dr}{\theta(r) \cdot r}\right)} \tag{4}$$

According to (2)–(4), the following relationships can be obtained

$$R_{leg} = f \cdot R_{leg,0} \tag{5a}$$

$$K_{leg} = \frac{K_{leg,0}}{f} \tag{5b}$$

$$f = \frac{\theta_0}{ln(Sr)} \int_{r_h}^{r_c} \frac{dr}{\theta(r) \cdot r} \tag{5c}$$

where f is defined as the shape factor. Hence, an algebraic relationship exists between the resistances and thermal conductances of *PN* legs of the VATEG and the CATEG, i.e., $K_{leg}R_{leg} = R_{leg,0}K_{leg,0}$. It can be seen that the CATEG can be considered a particular VATEG with $\theta(r) = \theta_0$ and $f = 1$.

In order to investigate the characteristics of VATEG based on the shape factor, it is expected that the integral in (5c) can be expressed analytically. Hence, in the following investigation, we limit our discussion to a special form of $\theta(r)$ so that the performance of the designed system can be analyzed both quantitatively and qualitatively.

2.2. Analysis of PN leg

Here, a two-parameter angle function is introduced to represent $\theta(r)$, i.e.,

$$\theta(r) = q \cdot r^m \tag{6}$$

where $q > 0$ and m are the scaling coefficient and the exponent coefficient, respectively. A reasonable range of m for practical design is $-2 \leqslant m \leqslant 2$. Using (1), (2), and (6), the scaling coefficient q can be expressed as a function of m, *Sr*, the angle θ_0 of the corresponding CATEG, as well as the inner radius r_h, i.e.,

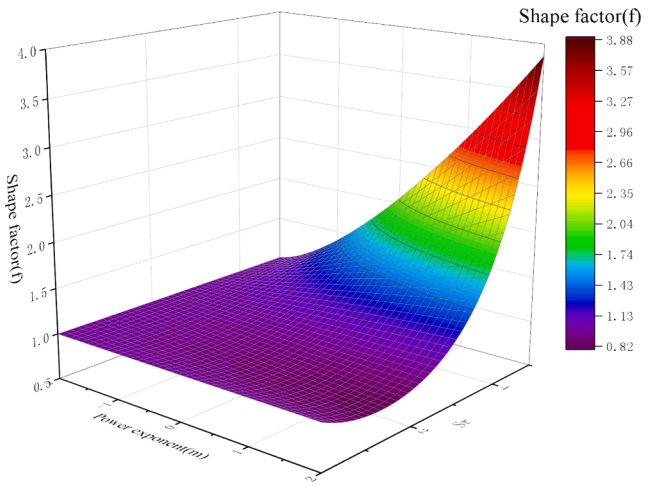

Fig. 3. Surface of the radius ratio *Sr* as a function of the coefficient *m* and the shape factor *f* for a VATEG.

$$q = \begin{cases} \dfrac{\theta_0 \cdot r_h^2 \cdot (Sr^2 - 1)}{2 \cdot ln(Sr)}, & m = -2 \\ \dfrac{(m+2) \cdot \theta_0 \cdot (Sr^2 - 1)}{2 \cdot r_h^m \cdot (Sr^{m+2} - 1)}, & m \neq -2 \end{cases} \tag{7}$$

Using (1), (2), and (5c), the shape factor f can be expressed as,

$$f = \begin{cases} 1, & m \in \{-2, 0\} \\ \dfrac{2 \cdot (Sr^m - 1) \cdot (Sr^{m+2} - 1)}{m \cdot (m+2) \cdot ln(Sr) \cdot Sr^m \cdot (Sr^2 - 1)}, & m \in (-2, 0) \cup (0, 2] \end{cases} \tag{8}$$

where f is a function of m and *Sr*, whereas θ_0 and r_h do not influence f. According to (8), the relationship between f, *Sr*, and m is plotted in Fig. 3, where it can be found that within the typical design range ($1 \leq Sr \leq 3.5$), one can increase f by increasing *Sr* or m. If f is less than 1, the resistance of the *PN* leg of CATEG ($m = 0$) is higher than that of VATEG, and the thermal conductance of CATEG is lower than that of VATEG. Fig. 4 presents the geometric relationships of *PN* leg in the polar coordinate with different m.

2.3. Boundary conditions

As observed in [51], the effect of geometric parameters on output performance also relies on the boundary conditions (BCs) on both sides of *PN* legs. This work considers three BCs, namely the constant temperature, constant heat flux, as well as constant convection heat transfer coefficient conditions, respectively. The three BCs are used for the cold and hot ends of the *PN* leg to solve the distributed temperature fields and to study the heat transfer process. Generally, we name the ceramic surface in direct contact with the heat source as the *hot side surface*, and the corresponding end of the *PN* leg is the *hot end*. On the other side, the surface in direct contact with the cold side radiator is called the *cold side surface*, and the corresponding end of the *PN* leg is the *cold end*.

2.3.1. Condition 1: Constant temperature on both sides

In Condition 1, the temperatures of both ends of *PN* legs maintain constant. As shown in Fig. 1(b), when T_1 and T_2 are kept constant, according to the 1D steady-state heat transfer equation, the heat absorbed by the hot end and the heat released from the cold end of a pair of *PN* legs can be expressed by [50]

$$Q_{in} = (\alpha_P - \alpha_N) \cdot I \cdot T_h + (K_P + K_N) \cdot (T_h - T_c) - 0.5 \cdot I^2 \cdot (R_N + R_P)$$
$$Q_{out} = (\alpha_P - \alpha_N) \cdot I \cdot T_c + (K_P + K_N) \cdot (T_h - T_c) + 0.5 \cdot I^2 \cdot (R_N + R_P) \tag{9}$$

where I is current, α is the Seebeck coefficient, K is thermal conductance,

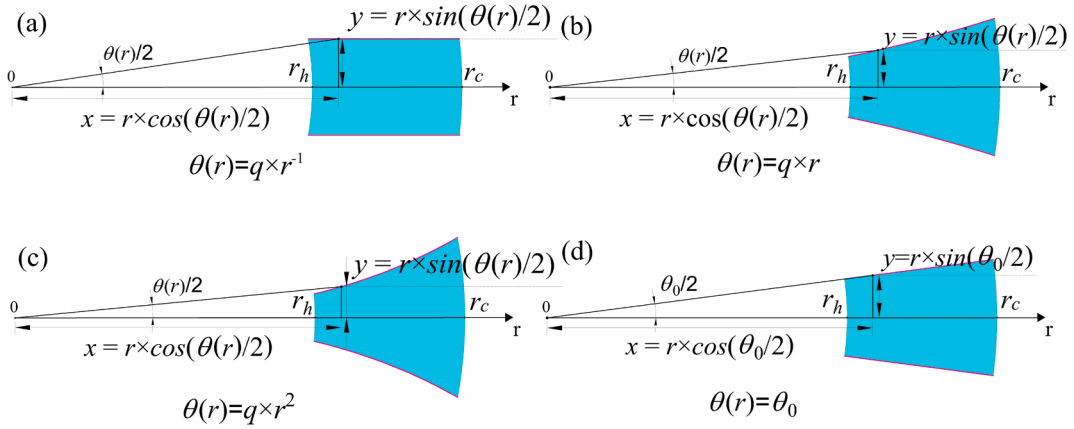

Fig. 4. Geometic relationships of *PN* legs of a VATEG with (a) $m = -1$, (b) $m = 1$, (c) $m = 2$, and (d) $m = 0$.

and the subscripts P and N denote the P-type and the N-type legs of VATEG, respectively.

By ignoring the effects of the thermal and electrical contact resistances, Q_{in} and Q_{out} can be expressed as

$$\begin{aligned} Q_{in} &= Q_1 = K_{1e}(T_1 - T_h) \\ Q_{out} &= Q_2 = K_{2e}(T_c - T_2) \end{aligned} \tag{10}$$

where K_{1e} and K_{2e} are the thermal conductances of the connection layers on the cold end and the hot end, respectively. Q_1 and Q_2 are the heat absorbed and released on the cold end and hot end, respectively. Hence, the temperatures at the two ends are

$$\begin{aligned} T_h &= T_1 - \frac{Q_{in}}{K_{1e}} \\ T_c &= T_2 + \frac{Q_{out}}{K_{2e}} \end{aligned} \tag{11}$$

Since the amount of heat absorbed by a single pair of *PN* legs is small, we assume $K_{1e} \gg Q_{in}$ and $K_{2e} \gg Q_{out}$, which gives

$$T_h \approx T_1, T_c \approx T_2 \tag{12}$$

Consequently, the Seebeck voltage U and the current I of *PN* legs in the VATEG can be obtained as

$$U \approx U_0 \approx (\alpha_P - \alpha_N)\cdot(T_h - T_c) \tag{13}$$

$$I = \frac{U}{R_t + R_L} \tag{14}$$

where $R_t = R_P + R_N$ is the internal resistance, and R_L is the external load. By combining (13) and (14) with (5), the relationship between the output performance of CATEG and VATEG can be established, i.e.,

$$I = \frac{U}{2\cdot R_t} = \frac{U_0}{2\cdot f\cdot R_{t0}} = \frac{I_0}{f} \tag{15}$$

$$P = U\cdot I = U_0\cdot\frac{I_0}{f} = \frac{P_0}{f} \tag{16}$$

$$\begin{aligned} \eta &= \frac{P}{Q_{in}} = \frac{P}{\alpha\cdot I\cdot T_h + K\cdot(T_h - T_c) - 0.5\cdot I^2\cdot R} \\ \eta_0 &= \frac{P_0/f}{\alpha\cdot(I_0/f)\cdot T_h + (K/f)\cdot(T_h - T_c) - 0.5\cdot(I_0/f)^2\cdot(R\cdot f)} \end{aligned} \tag{17}$$

$$\eta = \eta_0 \tag{18}$$

where $K = K_N + K_P$ and $\alpha = \alpha_N + \alpha_P$.

For the ease of performance evaluation and comparison between different models and designs, we define the *power ratio* P/P_0 and the *efficiency ratio* η/η_0. Clearly, under Condition 1, $P/P_0 = 1/f$ and $\eta/\eta_0 = 1$.

2.3.2. Condition 2: Constant heat flux on the hot side and constant temperature on the cold side

In this condition, Q_1 and T_2 shown in Fig. 1 are constant. Considering that the Seebeck coefficient of the *PN* leg is small (in the order of 10^{-4}), the first and third terms on the RHS of (9) can be neglected, which gives

$$K\cdot(T_h - T_c) = K_0\cdot(T_{h0} - T_{c0}) \tag{19}$$

The relationship between the temperature difference of VATEG and the temperature difference of CATEG is

$$T_h - T_c = f\cdot(T_{h0} - T_{c0}) \tag{20}$$

The output of the VATEG can be obtained as

$$P = \frac{(\alpha_P - \alpha_N)^2\cdot(T_h - T_c)^2}{4\cdot R_t} = \frac{f^2\cdot(\alpha_P - \alpha_N)^2\cdot(T_{h0} - T_{c0})^2}{4\cdot f\cdot R_{t0}} \tag{21}$$

$$P = f\cdot P_0 \tag{22}$$

$$\eta = f\cdot\eta_0 \tag{23}$$

Under Condition 2, the power ratio and the efficiency ratio are $P/P_0 = \eta/\eta_0 = 1/f$.

2.3.3. Condition 3: Constant convection coefficient on the hot side and constant temperature on the cold side

In this condition, the heat on the hot side of VATEG and CATEG can be expressed as

$$\begin{cases} Q_1 = \dfrac{(hA)\cdot K_{1e}}{hA + K_{1e}}\cdot(T_e - T_h) \\ Q_{10} = \dfrac{(hA)\cdot K_{1e}}{hA + K_{1e}}\cdot(T_e - T_{h0}) \end{cases} \tag{24}$$

where Q_1 and Q_{10} are the heat absorbed by the *PN* leg of VATEG and CATEG, respectively. h and T_e are the convective heat transfer coefficient and ambient temperature, respectively. A is the contact area between the hot side ceramic layer and the external heat fluid. Considering that $(K_P + K_N)\cdot(T_h - T_c) \gg (\alpha_P - \alpha_N)\cdot I\cdot T_h$ and $0.5\cdot I^2\cdot(R_N + R_P) \approx 0$, we have

$$\begin{aligned} Q_1 = Q_{in} &\approx Q_{out} \approx (K_P + K_N)\cdot(T_h - T_c) \\ Q_{10} = Q_{in0} &\approx Q_{out0} \approx (K_{P0} + K_{N0})\cdot(T_{h0} - T_{c0}) \end{aligned} \tag{25}$$

With (10), (24), and (25), the temperature difference between the two ends of *PN* legs is governed by

$$T_e - T_2 = (T_h - T_c)\cdot(1 + K\cdot C) \tag{26}$$

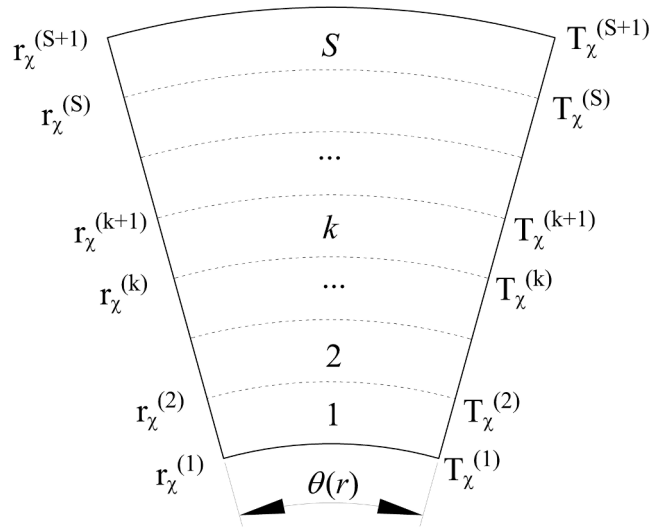

Fig. 5. Finite element analysis for a *PN* leg of VATEG. The *PN* leg is discretized into *S* elementary units in the radial direction.

where the $C = (\frac{1}{K_{1e}} + \frac{1}{K_{2e}} + \frac{1}{hA})$.

Similarly, for the CATEG,

$$T_e - T_2 = (T_{h0} - T_{c0})\cdot(1 + K_0\cdot C) \tag{27}$$

Hence, the relationship between the output powers, absorbed heat by the hot end, and efficiency of CATEG and VATEG are as follows, i.e.,

$$\frac{P}{P_0} = f\cdot\left(\frac{1 + K_0C}{f + K_0C}\right)^2 \tag{28}$$

$$\frac{Q_{in}}{Q_{in,0}} = \frac{1 + K_0C}{f + K_0C} \tag{29}$$

$$\frac{\eta}{\eta_0} = \frac{P/Q_{in}}{P_0/Q_{in0}} = f\cdot\frac{1 + K_0C}{f + K_0C} \tag{30}$$

2.4. Finite element analysis

Due to the highly nonlinear nature of the model and the coupled relationship between the properties and the temperature distribution of *PN* legs, an analytical solution of the model does not exist. Hence, an iterative numerical method based on FEM will be adopted to analyze the performance of VATEG. The schematic diagram of the finite element analysis of a single *PN* leg is shown in Fig. 5, where the *PN* leg is discretized into *S* elementary units. The subscript χ can be *P* or *N*, and *k* is the index of the elementary unit after discretization.

The physical parameters of each elementary unit can be calculated by

$$\alpha_\chi^{(k)} = \frac{\int_{T_\chi^{(k+1)}}^{T_\chi^{(k)}} \alpha_\chi dT}{T_\chi^{(k)} - T_\chi^{(k+1)}}, \lambda_\chi^{(k)} = \lambda_\chi(T)\Big|_{T=\frac{T_\chi^{(k)} - T_\chi^{(k+1)}}{2}}, \rho_\chi^{(k)} = \rho_\chi(T)\Big|_{T=\frac{T_\chi^{(k)} - T_\chi^{(k+1)}}{2}} \tag{31}$$

Using (4), the thermal conductance and the resistance of each elementary unit can be obtained, i.e.,

$$K_\chi^{(k)} = \frac{1}{\int_{r_\chi^{(k)}}^{r_\chi^{(k+1)}} \frac{dr}{\lambda_\chi^{(k)}\cdot\theta(r)\cdot r\cdot\delta}} \tag{32}$$

$$R_\chi^{(k)} = \int_{r_\chi^{(k)}}^{r_\chi^{(k+1)}} \frac{\rho_\chi^{(k)} dr}{\theta(r)\cdot r\cdot\delta} \tag{33}$$

The internal resistance and the Seebeck voltage of *PN* legs are

$$R_t = \sum_{k=1}^{S} R_\chi^{(k)} \tag{34}$$

$$U = \sum_{k=1}^{S} \alpha_\chi^{(k)}(T_\chi^{(k)} - T_\chi^{(k+1)}) \tag{35}$$

Since a thermoelectric module consists of *n* pairs of *PN* legs connected in series, the heat absorbed on the hot side and the heat released on the cold side can be expressed as

$$\begin{aligned} Q_{in} &= n\cdot(\alpha_\chi^{(1)} I T_h + K_\chi^{(1)}(T_\chi^{(1)} - T_\chi^{(2)}) - \frac{1}{2} I R_\chi^{(1)}\cdot R_\chi^{(1)}) \\ Q_{out} &= n\cdot(\alpha_\chi^{(S)} I T_c + K_\chi^{(S)}(T_\chi^{(S)} - T_\chi^{(S+1)}) + \frac{1}{2} I R_\chi^{(S)}\cdot R_\chi^{(S)}) \end{aligned} \tag{36}$$

where $\alpha_\chi = \alpha_P - \alpha_N$, $T_h = T_\chi^{(1)}$, $T_c = T_\chi^{(S+1)}$.

It should be noted that in order to obtain *I*, *P*, and η, the temperature distribution of *PN* legs must be given. In order to obtain the temperature distribution, we consider the following continuity of heat flow for a *PN* leg, i.e.,

$$\begin{aligned} &\alpha_\chi^{(k-1)} I T_\chi^{(k)} + K_\chi^{(k-1)}(T_\chi^{(k-1)} - T_\chi^{(k)}) + \frac{1}{2} I R_\chi^{(k-1)}\cdot R_\chi^{(k-1)} \\ &= \alpha_\chi^{(k)} I T_\chi^{(k)} + K_\chi^{(k)}(T_\chi^{(k)} - T_\chi^{(k+1)}) - \frac{1}{2} I R_\chi^{(k)}\cdot R_\chi^{(k)} \end{aligned} \tag{37}$$

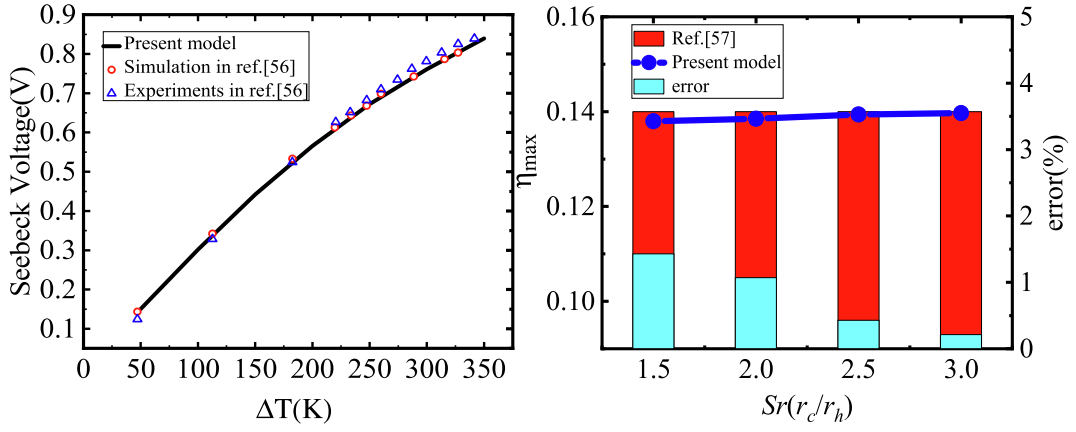

Fig. 6. Model validation. (a) Comparison between the simulated Seebeck voltage and experimental data from [56]. (b) Comparison between simulated maximum efficiency and experimental data from [57].

Table 1
Parameters of *PN* legs of the VATEG [58].

	P-type Semiconductor	N-type Semiconductor
$\alpha(V/K)$	$\alpha_p = -4.9\times10^{-16}T^4 + 9.17\times10^{-13}T^3 - 3.2\times10^{-9}T^2 + 2.3\times10^{-6}T - 2.6\times10^{-4}$	$\alpha_n = 1.36\times10^{-15}T^4 - 2.5\times10^{-12}T^3 + 2.94\times10^{-9}T^2 - 1.5\times10^{-6}T + 7.4\times10^{-5}$
$\lambda\ (W{\cdot}m^{-1}K^{-1})$	$\lambda_p = 3.04\times10^{-10}T^4 - 3.89\times10^{-7}T^3 + 2\times10^{-4}T^2 - 5.12\times10^{-2}T + 6.925$	$\lambda_n = -7.6\times10^{-11}T^4 + 1.12\times10^{-7}T^3 - 5.162\times10^{-5}T^2 + 6.51\times10^{-3}T + 1.426$
$\rho(\Omega/m)$	$\rho_p = -1.9\times10^{-16}T^4 + 3.47\times10^{-13}T^3 - 3.32\times10^{-10}T^2 + 1.97\times10^{-7}T - 2.85\times10^{-5}$	$\rho_n = -2.98\times10^{-16}T^4 + 4.92\times10^{-13}T^3 - 3.82\times10^{-10}T^2 + 1.79\times10^{-7}T - 1.96\times10^{-5}$
$n/r_h/\theta_0/\delta$	$1/3\ mm/\frac{\pi}{12}/1\ mm$	

Table 2
Boundary conditions and parameters [51,59].

Boundary Condition	Hot End	Cold End
Condition 1	$T_h = 403.15$ K	$T_c = 303.15$ K
Condition 2	$\xi = 30{,}000$ W m^{-2}	$T_c = 303.15$ K
Condition 3	$h = 3000$ W m^{-1} K^{-1} $T_e = 473.15$ K	$T_c = 303.15$ K

The temperature distribution of each elementary unit obtained in the iterative process can be described by

$$T_\chi^{(k)} = \frac{K_\chi^{(k-1)}T_\chi^{(k-1)} + K_\chi^{(k-1)}T_\chi^{(k+1)} + 0.5{\cdot}I(R_\chi^{(k-1)}R_\chi^{(k-1)} + R_\chi^{(k)}R_\chi^{(k)})}{(\alpha_\chi^{(k)} - \alpha_\chi^{(k-1)})I + K_\chi^{(k)} + K_\chi^{(k-1)}} \tag{38}$$

2.5. Model validation

The simulation and experimental results in Ref. [56] will be used to verify the accuracy of the proposed VATEG model. The design in [56] can be considered a particular case of the proposed model where the shape of *PN* legs is flat and the radius radio *Sr* is infinite. Fig. 6(a) compares the variation of the predicted voltages due to temperature change using the proposed VATEG model and the simulated and experimental data provided in [56]. The geometric parameters are the same as [56], and constant temperatures are considered on both sides (Condition 1). It can be seen that the maximum error between the experimental result and the result using the proposed method is less than 2%, and thus the model is deemed to reproduce the experimental results with high accuracy.

In addition, the output performance of the proposed model under constant temperature boundary conditions is verified using the data and parameters in Ref. [57] by controlling the temperature ratio T_h/T_c to 2. Fig. 6(b) shows the relationship between the maximum efficiency and the leg length using different models. It can be seen that that with the increase of leg length, the maximum efficiency varies slightly, and compared with the results in [57], the maximum error is only 1.5%. Therefore, this model is considered suitable for investigating the influence of leg shape on the output performance of the VATEG.

3. Results and discussion

In this section, the results from numerical analysis are presented based on the proposed VATEG model. Bi_2Te_3-based *PN* legs were investigated in this work. Bi_2Te_3 is a type of low/medium-temperature

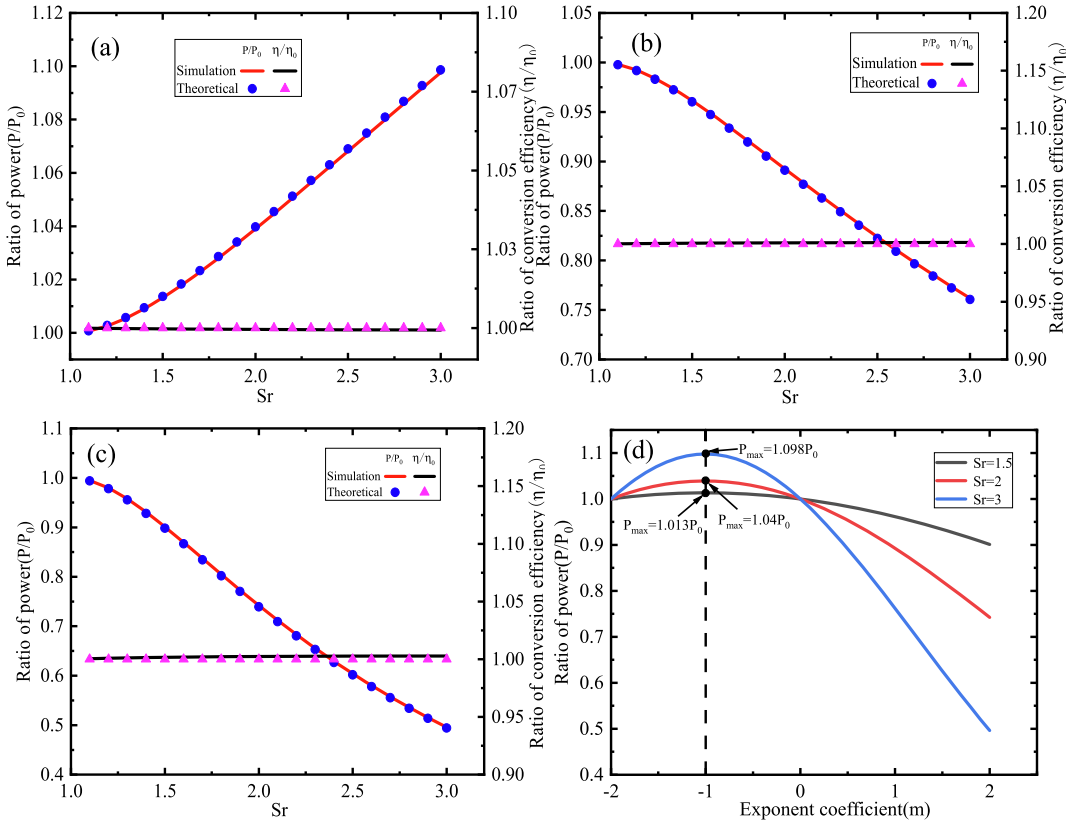

Fig. 7. Variations of power ratio P/P_0 and efficiency ratio η/η_0 with different exponent coefficient m under Conditions 1: (a) $m = -1$; (b) $m = 1$; (c) $m = 2$; (d) Variation of power ratio with m under different *Sr*.

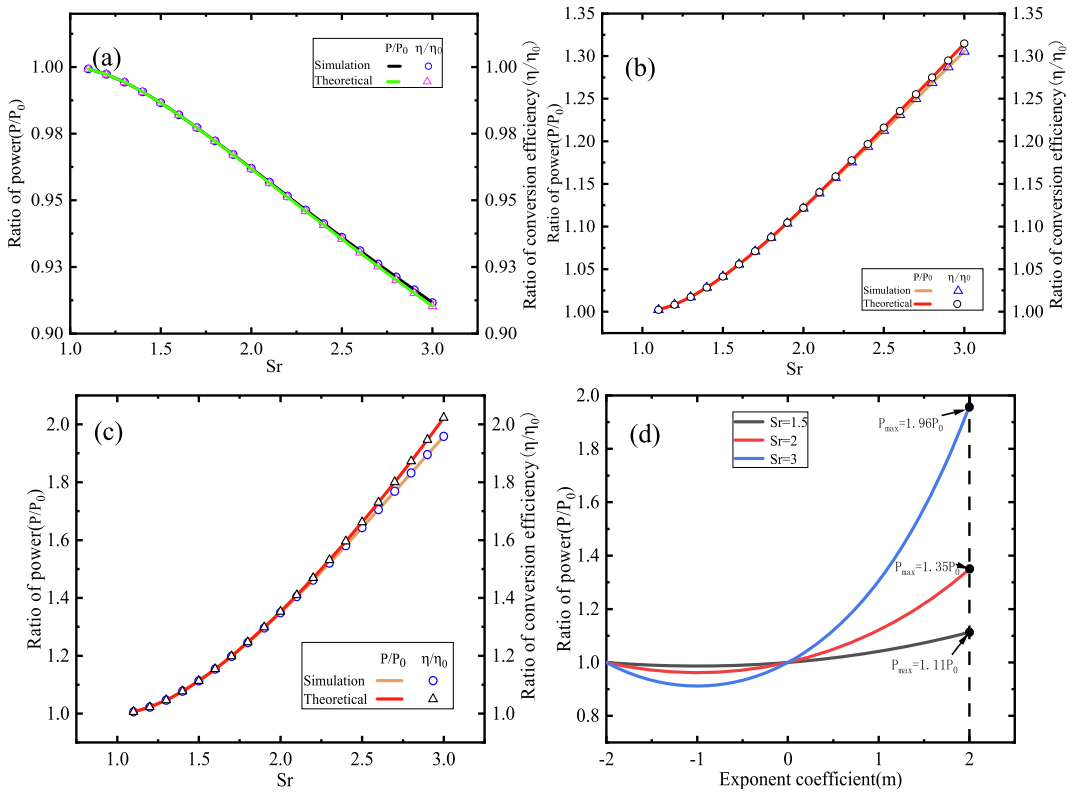

Fig. 8. Variations of power ratio P/P_0 and efficiency ratio η/η_0 with different exponent coefficient m under Conditions 2: (a) $m = -1$; (b) $m = 1$; (c) $m = 2$; (d) Variation of P/P_0 with m under different Sr.

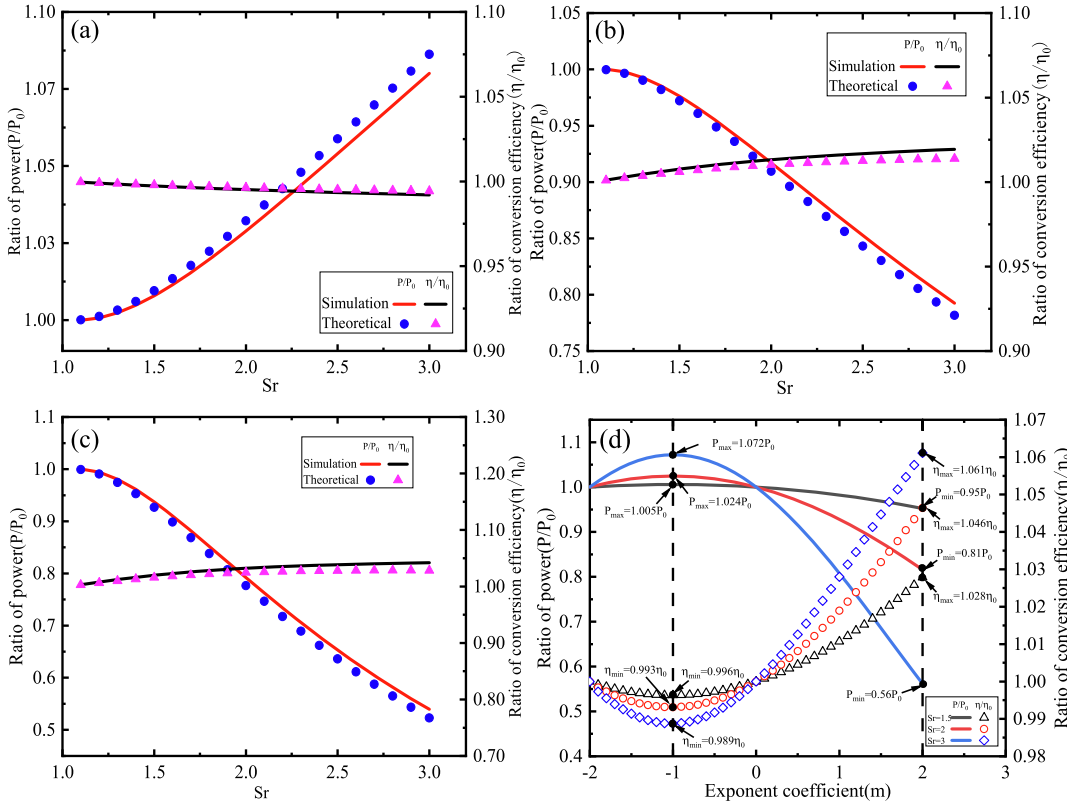

Fig. 9. Variations of power ratio P/P_0 and efficiency ratio η/η_0 with different exponent coefficient m under Conditions 3: (a) $m = -1$; (b) $m = 1$; (c) $m = 2$; (d) Variation of power ratio with m under different Sr.

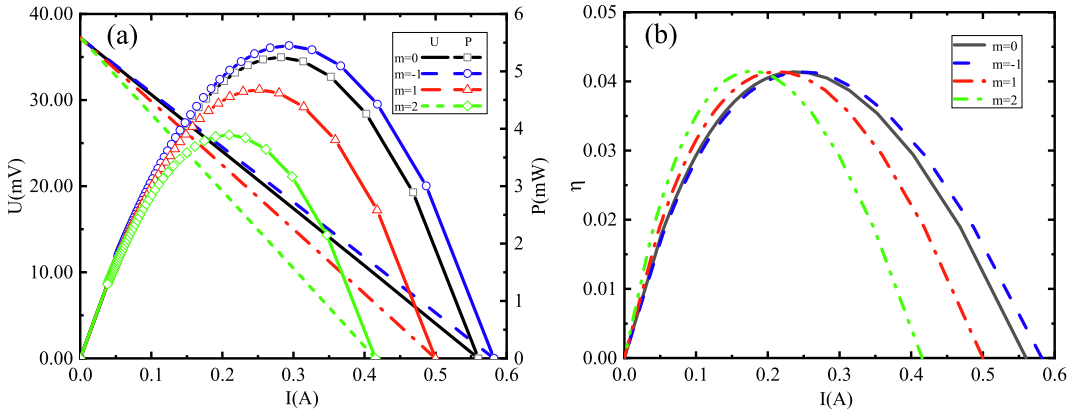

Fig. 10. Comparison of output performance under different *PN* legs angle shapes when $Sr = 2$ under Condition 1: *U–I* and *P–I* relationships. (b) η–*I* relationship.

thermoelectric material suited for the operating temperature ranging from 300 K to 500 K, and under this condition, the optimal performance can be obtained[58]. The model parameters are listed in Table 1. The simulated results were obtained using the proposed VATEG model and solved by the iterative numerical method in MATLAB.

3.1. Power ratio and efficiency ratio under different boundary conditions

Table 2 provides the parameters used for different BCs. Furthermore, the thermal conductivity and thickness of the ceramic layer are selected as $k_e = 30$ W/(m^2 K) and $r_e = 0.3$ mm. The thermal conductivity and thickness of the copper sheets are selected as $k_{Cu} = 400$ W/(m^2 K) and $r_{Cu} = 0.1$ mm. They were used to calculate the thermal conductances K_{e1} and K_{e2} of the connection layers in (10).

Under Condition 1, as illustrated in Fig. 7(a), the power ratio is over one at any leg length when $m = -1$. It implies that when the angle function of *PN* legs is in the form of qr^{-1}, higher output power can be achieved by the VATEG design compared to the CATEG regardless of leg length. With $m = -1$, a smaller shape factor f due to longer leg length would enhance the VATEG output power. Nevertheless, Fig. 7(b) and (c) show that if the angle function of the *PN* leg is qr or qr^2, the output power of CATEG is always optimal regardless of the selection of leg length.

On the other hand, the conversion efficiency is hardly affected by the leg shape under Condition 1. This can be explained using (16) and (18), from which it can be seen that the output power of VATEG is inversely proportional to the shape factor f. When $f < 1$ and $m = -1$, increasing the leg length would reduce f. Hence, the results on output performance obtained from theoretical analysis and finite element simulation are highly consistent. In addition, Fig. 7(d) shows the variation of power ratio with m under different Sr. It can be seen that when $m < 0$, the output power of VATEG is higher than that of CATEG, and the benefits using variable-angle leg can be maximized when $m = -1$. Compared to the CATEG, when $Sr = 1.5$, 2, and 3, the output power of VATEG can be increased by 1.3%, 4%, and 9.8%, respectively.

A similar analysis was carried out for Condition 2, and the results are shown in Fig. 8. It can be seen from Fig. 8 and explained using (22) and (23) that, with a constant heat flux Q_{in}, both the output power and the conversion efficiency can be increased by increasing the shape factor f. Furthermore, f can be increased with a higher Sr when $m > 0$, while it will be decreased when $m < 0$. It can be found that the assumption made in Section 2 for theoretical analysis has become less valid in the simulation where the leg length is long. Nevertheless, in practice, the assumption tends to be valid since a design with a long leg length should be avoided to maintain structural stability. A quantitative analysis of the influence of shape change on output performance was carried out, and the results are presented in Fig. 8(d). It is observed that when $m = 2$, the output performance of VATEG is maximized at any leg length. In terms of the output power, the performance of VATEG is 11% higher than that of CATEG when $Sr = 1.5$. The improvement in output power can be further increased with a higher Sr, e.g., 35% if $Sr = 2$, and 96% if $Sr = 3$.

Fig. 9(a)–(c) reveals the relationship between the power ratio, the efficiency ratio, and Sr with different *PN* leg shape factors m under Condition 3. It can be seen that the curves obtained from the theoretical analysis are again close to the simulation results based on the FEM. In Fig. 9(d), variations of the power and efficiency ratios with the change of m show opposite trends, which indicates they cannot be optimized simultaneously. Particularly, when $m = -1$, the output power of VATEG is maximized, whereas $m = -1$ is the least efficient operating condition. Furthermore, when $m = -1$, the output power can be improved by 7.2%, 2.4%, and 0.5%, respectively, when $Sr = 3$, 2, and 1.5, respectively, while the corresponding efficiency decreases by 1.1%, 0.7%, and 0.4%, respectively. When $m = 2$, the efficiency can be increased by 6.1%,

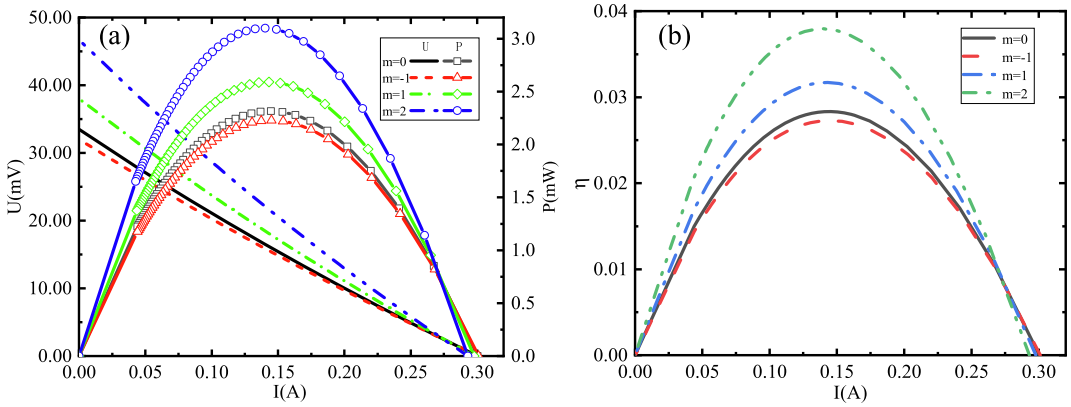

Fig. 11. Comparison of output performance under different *PN* legs angle shapes when $Sr = 2$ under Condition 2: (a) *U–I* and *P–I* relationships. (b) η–*I* relationship.

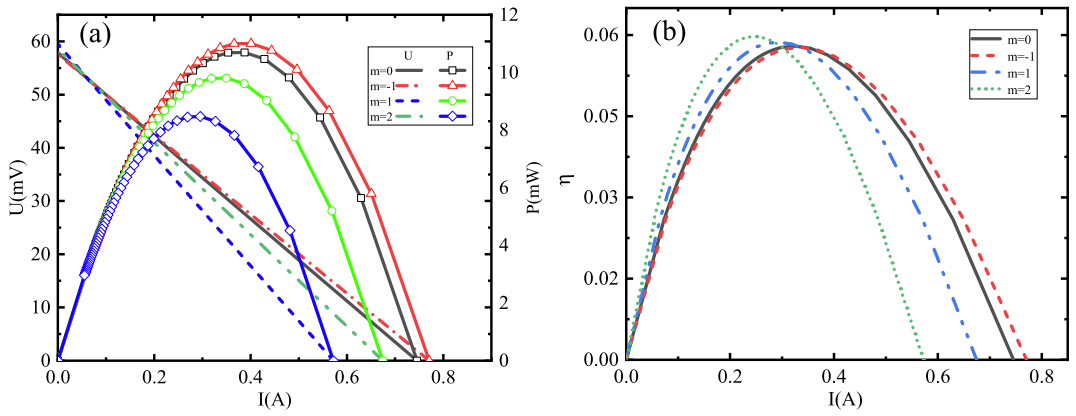

Fig. 12. Comparison of output performance under different *PN* legs angle shapes when $Sr = 2$ under Condition 3: (a) *U–I* and *P–I* relationships. (b) *η–I* relationship.

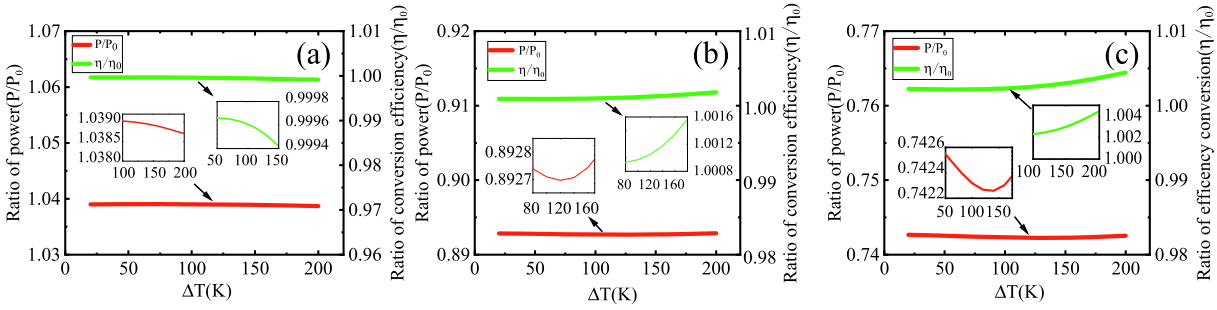

Fig. 13. Impacts of temperature difference on output performance with various shapes of *PN* legs under Condition 1. (a) $m = -1$. (b) $m = 1$. (c) $m = 2$.

4.6%, and 2.8%, respectively, whereas the output power is decreased by 44%, 19%, and 5%, respectively.

3.2. Comparison of output performance under different boundary conditions

Under Condition 2, although increasing the leg length can improve the output performance, a practical design shall also consider structural stability. For example, in the case of $m = 2$, with the increase of *Sr*, the angle of *PN* legs increases exponentially. Given a constant volume as the design requirement, the calculated hot side contact area of the *PN* leg will be very small if the leg length is long, leading to structural instability. Hence, a high radius radio such as $Sr = 3$ is not suitable for practical applications.

Figs. 10–12 compare the *U–I*, *P–I*, and *η–I* relationships under different BCs when $Sr = 2$. In Fig. 9, under Condition 1, the output power of a pair of *PN* legs in CATEG ($m = 0$) is 5.24 mW. In contrast, the VATEG can achieve the maximum power of 5.45 mW when $m = -1$, which is 4% higher than the CATEG. Also, the short-circuit current is the highest when $m = -1$, which is 0.59 A. Moreover, the OCV, i.e., the Seebeck voltage *U* when $I = 0$, is unchanged.

Fig. 11 illustrates the output performance under Condition 2. It can be seen that when $m = 2$, both the efficiency and the output power are significantly increased compared to CATEG: The maximum output power is 3.1 mW, and the maximum efficiency is 3.8%, increased by 34% and 2.8%, respectively. In contrast, the short-circuit current is hardly affected by the shape of *PN* legs. In addition, the shape factor affects the OCV, and the maximum OCV is obtained when $m = 2$.

Fig. 12 compares output performance under Condition 3. The maximum output power of the VATEG is 11 mW when $m = -1$, which is only 0.3 mW or 2.4% higher than the CATEG. In this case, the improvement in the performance is limited through modifying the leg shape.

3.3. Influence of external parameters on the performance of PN legs under different boundary conditions

In this subsection, we investigate the influence of external parameters on the output performance of the VATEG under different BCs when $Sr = 2$. Fig. 13 presents the relationship between the power ratio and the

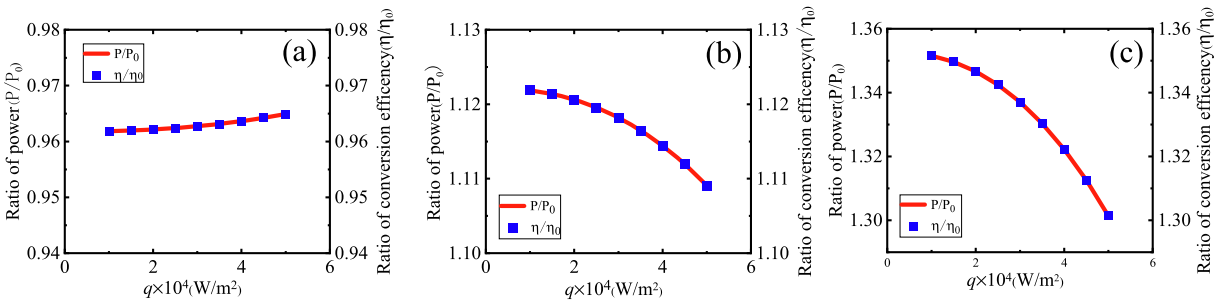

Fig. 14. Impacts of heat flux on output performance with various shapes of *PN* legs under Condition 2. (a) $m = -1$. (b) $m = 1$. (c) $m = 2$.

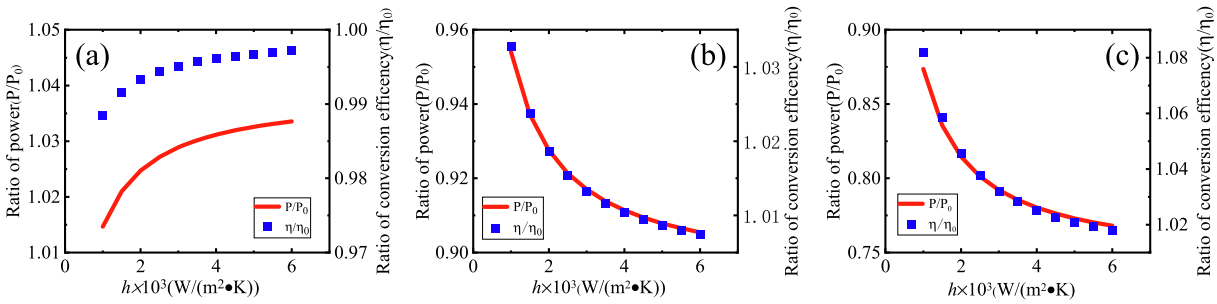

Fig. 15. Impacts of convective heat transfer coefficient on output performance with various shapes of *PN* legs under Condition 3. (a) $m = -1$. (b) $m = 1$. (c) $m = 2$.

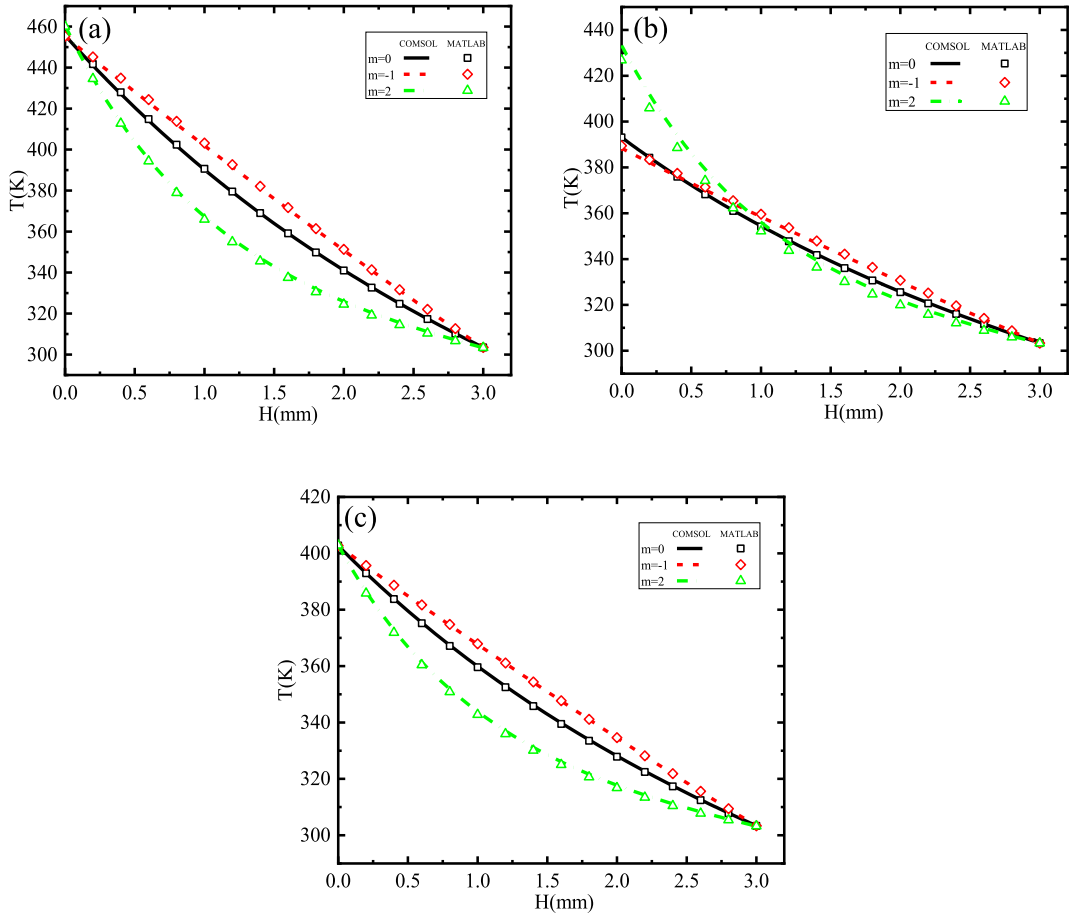

Fig. 16. Temperature distribution of *PN* legs with different shapes along the leg length direction. (a) Condition 1. (b) Condition 2. (b) Condition 3.

temperature difference with different m when the cold end temperature is fixed. It can be seen from the results that the change of temperature difference has little impact on the VATEG output power and efficiency regardless of the shape of *PN* legs. Therefore, the effect of temperature differences can be ignored in the design for practical applications.

Fig. 14 illustrates the influence of the heat flux on the output performance under Condition 2. It shows that the influence of heat flux on output performance depends heavily on the exponent coefficient m of the variable-angle *PN* legs. It can be seen that compared to Fig. 13, the influence of heat flux on the output performance is more significant. As the heat flux increases, there are different trends for different m. Specifically, when $m = -1$, the output performance can be improved by increasing the heat flux. In contrast, increasing the heat flux will cause reduced output power and efficiency when $m = 1$ or $m = 2$.The results show that although a design of *PN* leg shape with $m = 2$ can improve the output performance compared to the conventional ATEG, for a practical system, the heat flux must be limited to avoid reduced performance.

Fig. 15 shows the effect of the convective heat transfer coefficient h on the output performance of *PN* legs with different shapes under Condition 3. It can be seen that when the convective heat transfer coefficient varies from 1000 W/(m^2·K) to 6000 W/(m^2·K), the output power and the efficiency increase as h increases when $m = -1$, and thus this shape of *PN* leg can be used for high convective heat transfer coefficient. On the contrary, the output performance will deteriorate as h increases when $m = 1$ or $m = 2$, and thus the corresponding *PN* leg is only suitable for the operating conditions with low convective heat transfer coefficient.

3.4. Thermal stress analysis and temperature distribution of different PN leg shapes with COMSOL

As the material characteristics are related to temperature, the shape

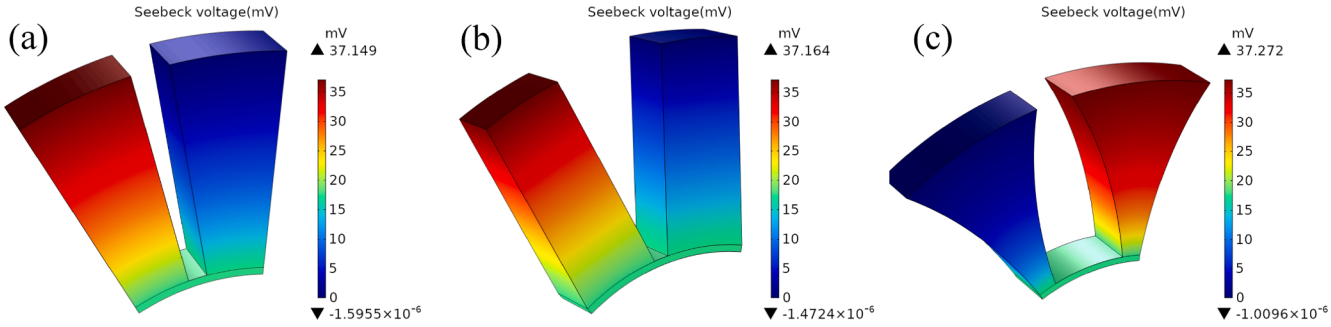

Fig. 17. Seebeck voltage of *PN* legs with different shapes under Condition 1. (a) $m = 0$ (CATEG). (b) $m = -1$. (c) $m = 2$.

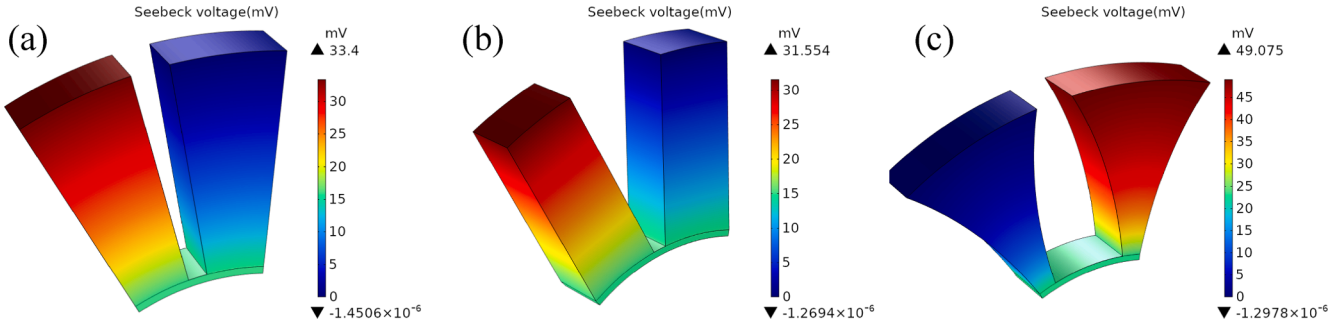

Fig. 18. Seebeck voltage of *PN* legs with different shapes under Condition 2. (a) $m = 0$ (CATEG). (b) $m = -1$. (c) $m = 2$.

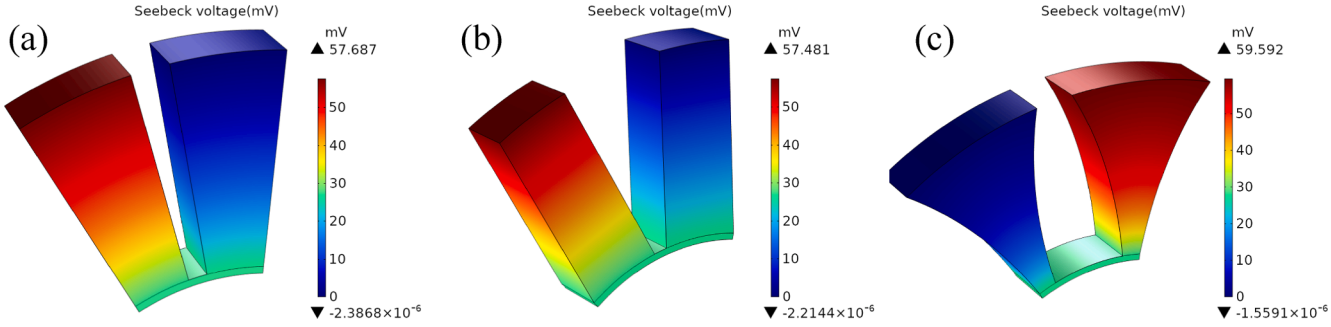

Fig. 19. Seebeck voltage of *PN* legs with different shapes under Condition 3. (a) $m = 0$ (CATEG). (b) $m = -1$. (c) $m = 2$.

of *PN* legs change would significantly affect the variation of the temperature distribution on *PN* legs. It is necessary to investigate the upper limit of the local temperature of the *PN* leg to avoid overheating problems. Fig. 16 compares the simulated temperature distributions of a *PN* leg in the leg length direction obtained from COMSOL and MATLAB when $Sr = 2$. The results show that the proposed algorithm based on finite element analysis is accurate with different VATEG designs. It can be seen that when $m = 2$, the nonlinearity of temperature distribution is significant under all boundary conditions, and only under Condition 2, the hot side temperature of *PN* legs will increase obviously in this shape, which is nearly 30 K higher than the hot side temperature of CATEG. This phenomenon can account for with the same leg volume, a smaller hot side contact cross-sectional area of *PN* legs at $m = 2$ would obstruct the thermal conductivity, which attributes to significant temperature

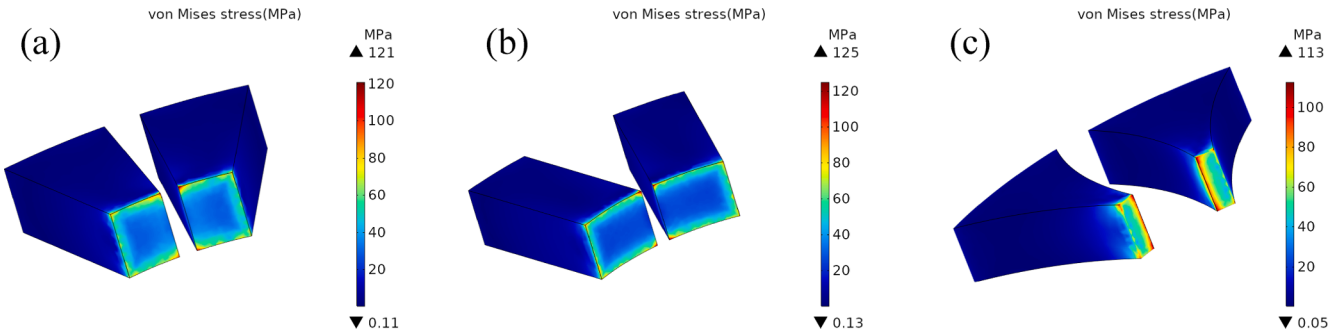

Fig. 20. Thermal stress of *PN* legs with different shapes under Condition 1: (a) $m = 0$ (CATEG). (b) $m = -1$. (c) $m = 2$.

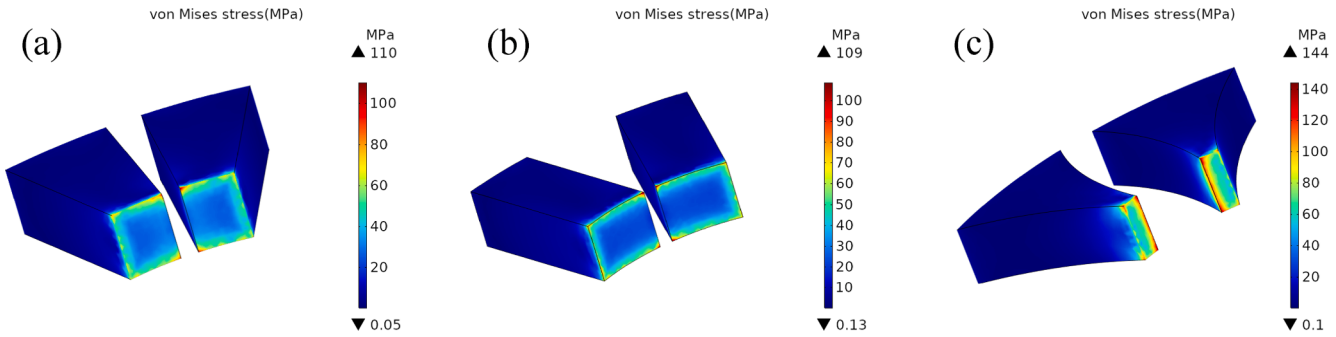

Fig. 21. Thermal stress of *PN* legs with different shapes under Condition 2: (a) $m = 0$ (CATEG). (b) $m = -1$. (c) $m = 2$.

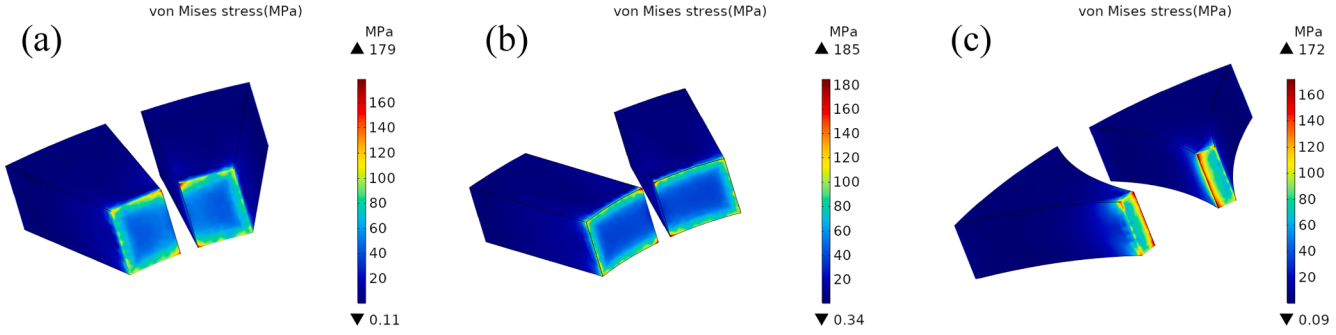

Fig. 22. Thermal stress of *PN* legs with different shapes under Condition 3. (a) $m = 0$ (CATEG). (b) $m = -1$. (c) $m = 2$.

differences along the *PN* legs. In conclusion, a suitable cross-section of *PN* legs can avoid excessive temperature rise and damaging the materials.

Figs. 17–19 illustrate the Seebeck voltage of *PN* legs obtained from COMSOL with different m and under different boundary conditions. Fig. 17 measures the Seebeck voltage under Condition 1. It can be observed that the maximum Seebeck voltage, i.e., the OCVs are all about 37 mV with different shapes, which is consistent with the results shown in Fig. 10(a). Similar results can be observed under Condition 3 as shown in Fig. 19: the OCVs are close, which complies with the results in Fig. 12. In contrast, under Condition 2, the OCVs are quite different with different *PN* legs. The OCV reaches up to 49.08 mV when $m = 2$, and this is 15.68 mV or 50% higher than the CATEG.

To investigate how the shape of the *PN* legs can affect the stability of thermoelectric materials, Figs. 20–22 show the thermal stress distribution of various *PN* legs under different BCs when $Sr = 2$. It is worth noting that the thermal stresses in all *PN* leg shapes are on the hot end of *PN* legs. Furthermore, it can be seen that the coefficient m has little impact on the thermal stress and the stability of the materials under the three applied BCs. Nevertheless, under Condition 2 as shown in Fig. 21, the thermal stress increases dramatically when $m = 2$ (about 31% compared to $m = 0$). This is mainly because a higher temperature can be achieved with this design at the hot end of the *PN* legs.

4. Conclusion

A variable-angle annular thermoelectric generator (VATEG) is proposed in this work. First, the relationship between the output performance of VATEG and a conventional constant-angle annular thermoelectric generator (CATEG) under three boundary conditions is investigated analytically and numerically, including constant temperature on both sides of the *PN* leg (Condition 1), constant heat flux on the hot side and constant temperature on the cold side (Condition 2), and constant convection coefficient on the hot side and constant temperature on the cold side (Condition 3). Several parameters are defined to indicate the geometrical characteristics of the VATEG, including shape factor f, radius ratio Sr, and exponent coefficient m. Next, the optimal output performance of VATEG is obtained with different radius ratios of *PN* legs. Finally, the open-circuit voltage and the thermal stress distribution of the *PN* legs are investigated through 3D simulation in COMSOL. The main findings of this work are summarized as follows.

(1) Boundary conditions can affect the output performance of the VATEG significantly. For example, under Condition 1, the maximum output power of the *PN* leg with variable leg angles is inversely proportional to the shape factor f, while the maximum conversion efficiency is not affected by the shape factor. Under Condition 2, the maximum output power and the maximum conversion efficiency of the *PN* legs with variable angles are proportional to f. Furthermore, the maximum output power is negatively correlated with f, while the corresponding conversion efficiency is positively correlated with f under Condition 3.

(2) The specific output performance of *PN* legs when $Sr = 2$ is analyzed. When $m = -1$, the output power reaches its maximum value, 4% higher than that of CATEG under Condition 1. The output power and conversion efficiency are 35% higher than CATEG under Condition 2 when $m = 2$, while the thermal stress increases by 31%. Under Condition 3, although the maximum output power of the VATEG is 2.4% higher than the CATEG, the conversion efficiency is slightly reduced.

(3) From theoretical analysis and numerical simulation, consistent temperature distributions are obtained in the radial direction of the *PN* leg. The hot side temperature will increase only under Condition 2 with $m = 2$, leading to an increase in the voltage.

(4) The impacts of the external environment on the output performance are investigated with various shapes of PN legs. The results show that the temperature difference has little influence on the output performance. However, heat flux and convective heat transfer coefficient greatly influence the output performance, and these two factors should be considered in practice.

(5) The performance of the VATEG is superior to the conventional CATEG in terms of output power and efficiency. Under

Conditions (1) and (3), the VATEG efficiency is 4% and 2.4% higher than CATEG, respectively, when $m = -1$. When $m = 2$, the efficiency and output power can be increased by 34% under Condition 2.

CRediT authorship contribution statement

Zebin Weng: Data curation, Writing – original draft. **Furong Liu:** Formal analysis, Methodology. **Wenchao Zhu:** Data curation, Investigation, Writing – original draft. **Yang Li:** Formal analysis, Writing – review & editing. **Changjun Xie:** Conceptualization, Funding acquisition, Project administration, Supervision, Writing – review & editing. **Jian Deng:** Investigation, Methodology, Validation. **Liang Huang:** Conceptualization, Project administration, Software, Validation.

Declaration of Competing Interest

The authors declare that they have no known competing financial interests or personal relationships that could have appeared to influence the work reported in this paper.

Acknowledgments

This research was supported by the National Key Research and Development Program of China (2020YFB1506802) and the National Natural Science Foundation of China (51977164).

References

[1] Li B, Huang K, Yan YY, Li Y, Twaha S, Zhu J. Heat transfer enhancement of a modularised thermoelectric power generator for passenger vehicles. Appl Energy 2017;205:868–79.
[2] Pourkiaei SM, Ahmadi MH, Sadeghzadeh M, Moosavi S, Pourfayaz F, Chen LE, et al. Thermoelectric cooler and thermoelectric generator devices: A review of present and potential applications, modeling and materials. Energy 2019;186.
[3] Fateh H, Baker CA, Hall MJ, Shi L. High fidelity finite difference model for exploring multi-parameter thermoelectric generator design space. Appl Energy 2014;129:373–83.
[4] Lan S, Yang ZJ, Chen R, Stobart R. A dynamic model for thermoelectric generator applied to vehicle waste heat recovery. Appl Energy 2018;210:327–38.
[5] Muthu G, Shanmugam S, Veerappan AR. Theoretical and Experimental Study on a Thermoelectric Generator Using Concentrated Solar Thermal Energy. J Electron Mater 2019;48.
[6] Tanwar A, Lal S, Razeeb KM. Structural Design Optimization of Micro-Thermoelectric Generator for Wearable Biomedical Devices. Energies 2021;14.
[7] Deng W, Wang XJ, Pan XD, Zhang SX, Ding JJ, Li GP. Geometry design and performance optimization of a terrestrial radioisotope thermoelectric generator based on finite element analysis. Ann Nucl Energy 2021;151.
[8] Nozariasbmarz A, Dycus JH, Cabral MJ, Flack CM, Krasinski JS, LeBeau JM, et al. Efficient self-powered wearable electronic systems enabled by microwave processed thermoelectric materials. Appl Energy 2021;283.
[9] Yang L, Chen ZG, Dargusch MS, Zou J. High Performance Thermoelectric Materials: Progress and Their Applications. Adv Energy Mater 2018:8.
[10] Xiwen Z, Chenhan L, Yi T, Yunhai L, Yilv G, Yunfei C, et al. High ZT 2D Thermoelectrics by Design: Strong Interlayer Vibration and Complete Band-Extrema Alignment. Adv Funct Mater 2020;30.
[11] Anh Tuan D, Van Quang N, Ganbat D, Van Thiet D, Suyong K, Jae Yong S, et al. Achieving ZT=2.2 with Bi-doped n-type SnSe single crystals. Nat Commun 2016;7.
[12] Zhao LD, Dravid VP, Kanatzidis MG. The panoscopic approach to high performance thermoelectrics. Energ Environ Sci 2014;7:251–68.
[13] Pei YZ, Shi XY, LaLonde A, Wang H, Chen LD, Snyder GJ. Convergence of electronic bands for high performance bulk thermoelectrics. Nature 2011;473:66–9.
[14] Yang JH, Caillat T. Thermoelectric materials for space and automotive power generation. Mrs Bull 2006;31:224–9.
[15] Ming X, M GD. Potential impact of ZT = 4 thermoelectric materials on solar thermal energy conversion technologies. J Phys Chem. B 2010;114.
[16] Jood P, Mehta RJ, Zhang YL, Peleckis G, Wang XL, Siegel RW, et al. Al-Doped Zinc Oxide Nanocomposites with Enhanced Thermoelectric Properties. Nano Lett 2011;11:4337–42.
[17] Gnanaseelan M, Samanta S, Pionteck J, Jehnichen D, Simon F, Potschke P, et al. Vanadium salt assisted solvothermal reduction of graphene oxide and the thermoelectric characterisation of the reduced graphene oxide in bulk and as composite. Mater Chem Phys 2019;229:319–29.
[18] Rogl G, Ghosh S, Renk O, Yubuta K, Grytsiv A, Schafler E, et al. Influence of shear strain on HPT-processed n-type skutterudites yielding ZT=2.1. J Alloy Compd 2020.
[19] Zhao LD, Tan GJ, Hao SQ, He JQ, Pei YL, Chi H, et al. Ultrahigh power factor and thermoelectric performance in hole-doped single-crystal SnSe. Science 2016;351:141–4.
[20] Shuai J, Mao J, Song S, Zhang Q, Chen G, Ren Z. Recent progress and future challenges on thermoelectric Zintl materials. Mater Today Phys 2017;1.
[21] Rogl G, Yubuta K, Romaka VV, Michor H, Schafler E, Grytsiv A, et al. High-ZT half-Heusler thermoelectrics, Ti 0.5 Zr 0.5 NiSn and Ti 0.5 Zr 0.5 NiSn 0.98 Sb 0.02: Physical properties at low temperatures. Acta Mater 2018;166.
[22] Ma X, Shu G, Tian H, Xu W, Chen T. Performance assessment of engine exhaust-based segmented thermoelectric generators by length ratio optimization. Appl Energy 2019;248.
[23] Atouei SA, Ranjbar AA, Rezania A. Experimental investigation of two-stage thermoelectric generator system integrated with phase change materials. Appl Energy 2017;208:332–43.
[24] Chen WH, Chiou YB. Geometry design for maximizing output power of segmented skutterudite thermoelectric generator by evolutionary computation. Appl Energy 2020;274.
[25] Karana DR, Sahoo RR. Influence of geometric parameter on the performance of a new asymmetrical and segmented thermoelectric generator. Energy 2019;179:90–9.
[26] El-Genk MS, Saber HH, Caillat T. Efficient segmented thermoelectric unicouples for space power applications. Energy Convers Manage 2003;44:1755–72.
[27] Massaguer A, Massaguer E, Comamala M, Pujol T, Gonzalez JR, Cardenas MD, et al. A method to assess the fuel economy of automotive thermoelectric generators. Appl Energy 2018;222:42–58.
[28] Meng FK, Chen LG, Sun FR. A numerical model and comparative investigation of a thermoelectric generator with multi-irreversibilities. Energy 2011;36:3513–22.
[29] Wang XD, Huang YX, Cheng CH, Lin DTW, Kang CH. A three-dimensional numerical modeling of thermoelectric device with consideration of coupling of temperature field and electric potential field. Energy 2012;47:488–97.
[30] Wang YP, Li S, Xie X, Deng YD, Liu X, Su CQ. Performance evaluation of an automotive thermoelectric generator with inserted fins or dimpled-surface hot heat exchanger. Appl Energy 2018;218:391–401.
[31] Bauknecht A, Steinert T, Spengler C, Suck G. Analysis of Annular Thermoelectric Couples with Nonuniform Temperature Distribution by Means of 3-D Multiphysics Simulation. J Electron Mater 2013;42:1641–6.
[32] Shen ZG, Wu SY, Xiao L. Assessment of the performance of annular thermoelectric couples under constant heat flux condition. Energy Convers Manage 2017;150:704–13.
[33] Hongliu D, Gaixia Z, Diane R, Chaoying F, Chao W, Xianhu L, et al. Polymer gel electrolytes for flexible supercapacitors: Recent progress, challenges, and perspectives. Energy Storage Mater 2021;34.
[34] C YJ, W BL, W KF. Energy conversion performance optimization and strength evaluation of a wearable thermoelectric generator made of a thermoelectric layer on a flexible substrate. Energy 2021;229.
[35] Kim TY, Negash A, Cho G. Direct contact thermoelectric generator (DCTEG): A concept for removing the contact resistance between thermoelectric modules and heat source. Energy Convers Manage 2017;142.
[36] Asaadi S, Khalilarya S, Jafarmadar S. Numerical study on the thermal and electrical performance of an annular thermoelectric generator under pulsed heat power with different types of input functions. Energy Convers Manage 2018;167:102–12.
[37] Fan SF, Gao YW. Numerical analysis on the segmented annular thermoelectric generator for waste heat recovery. Energy 2019;183:35–47.
[38] Shittu S, Li GQ, Zhao XD, Ma XL, Akhlaghi YG, Ayodele E. Optimized high performance thermoelectric generator with combined segmented and asymmetrical legs under pulsed heat input power. J Power Sources 2019;428:53–66.
[39] Shittu S, Li GQ, Zhao XD, Ma XL, Akhlaghi YG, Ayodele E. High performance and thermal stress analysis of a segmented annular thermoelectric generator. Energy Convers Manage 2019;184:180–93.
[40] Liu ZC, Zhu SP, Ge Y, Shan F, Zeng LP, Liu W. Geometry optimization of two-stage thermoelectric generators using simplified conjugate-gradient method. Appl Energy 2017;190:540–52.
[41] Chen WH, Huang SR, Lin YL. Performance analysis and optimum operation of a thermoelectric generator by Taguchi method. Appl Energy 2015;158:44–54.
[42] Chen WH, Wu PH, Lin YL. Performance optimization of thermoelectric generators designed by multi-objective genetic algorithm. Appl Energy 2018;209:211–23.
[43] Fan L, Zhang G, Wang R, Jiao K. A comprehensive and time-efficient model for determination of thermoelectric generator length and cross-section area. Energy Convers Manage 2016;122.
[44] He H, Wu Y, Liu W, Rong M, Fang Z, Tang X. Comprehensive modeling for geometric optimization of a thermoelectric generator module. Energy Convers Manage 2019;183.
[45] Fabian-Mijarigos A, Min G, Alvarez-Quintana J. Enhanced performance thermoelectric module having asymmetrical legs. Energy Convers Manage 2017;148:1372–81.
[46] Sahin AZ, Yilbas BS. The thermoelement as thermoelectric power generator: Effect of leg geometry on the efficiency and power generation. Energy Convers Manage 2013;65:26–32.
[47] Yilbas BS, Ali H. Thermoelectric generator performance analysis: Influence of pin tapering on the first and second law efficiencies. Energy Convers Manage 2015;100:138–46.
[48] Niu ZQ, Yu SH, Diao H, Li QS, Jiao K, Du Q, et al. Elucidating modeling aspects of thermoelectric generator. Int J Heat Mass Tran 2015;85:12–32.

[49] Sisik B, LeBlanc S. The Influence of Leg Shape on Thermoelectric Performance Under Constant Temperature and Heat Flux Boundary Conditions. Front Mater 2020;7.
[50] Zhang AB, Wang BL, Pang DD, Chen JB, Wang J, Du JK. Influence of leg geometry configuration and contact resistance on the performance of annular thermoelectric generators. Energy Convers Manage 2018;166:337–42.
[51] Liu HB, Wang SL, Yang YR, Chen WH, Wang XD. Theoretical analysis of performance of variable cross-section thermoelectric generators: Effects of shape factor and thermal boundary conditions. Energy 2020:201.
[52] Ali H, Sahin AZ, Yilbas BS. Thermodynamic analysis of a thermoelectric power generator in relation to geometric configuration device pins. Energy Convers Manage 2014;78:634–40.
[53] Liu HB, Meng JH, Wang XD, Chen WH. A new design of solar thermoelectric generator with combination of segmented materials and asymmetrical legs. Energy Convers Manage 2018;175:11–20.
[54] Yilbas BS, Akhtar SS, Sahin AZ. Thermal and stress analyses in thermoelectric generator with tapered and rectangular pin configurations. Energy 2016;114:52–63.
[55] Shen ZG, Wu SY, Xiao L, Yin G. Theoretical modeling of thermoelectric generator with particular emphasis on the effect of side surface heat transfer. Energy 2016;95:367–79.
[56] Ebling D, Jaegle M, Bartel M, Jacquot A, Bottner H. Multiphysics Simulation of Thermoelectric Systems for Comparison with Experimental Device Performance. J Electron Mater 2009;38:1456–61.
[57] Shen ZG, Wu SY, Xiao L. Theoretical analysis on the performance of annular thermoelectric couple. Energy Convers Manage 2015;89:244–50.
[58] Ding L, Ruochen W, Wei Y, Zeyu S, Meng Xiangpeng. Theoretical analysis of energy recovery potential for different types of conventional vehicles with a thermoelectric generator. Energy Proc 2019;158.
[59] Nozariasbmarz A, Poudel B, Li W, Kang HB, Zhu H, Priya S. Bismuth telluride thermoelectrics with 8% module efficiency for waste heat recovery application. iScience 2020;23:101340.